ELSEVIER

Polymer 42 (2001) 9133–9141

polymer

www.elsevier.com/locate/polymer

Interfacial properties of elastomer blends as studied by neutron reflectivity

Yimin Zhang[a], W. Li[a], B. Tang[a], S. Ge[a], X. Hu[a], M.H. Rafailovich[a], J.C. Sokolov[a], D. Gersappe[a], D.G. Peiffer[b,*], Z. Li[b], A.J. Dias[c], K.O. McElrath[c], M.Y. Lin[d], S.K. Satija[d], S.G. Urquhart[e,1], H. Ade[e]

[a]*Department of Materials Science and Engineering, State University of New York at Stony Brook, Stony Brook, NY 11794, USA*
[b]*ExxonMobil Research and Engineering Company, Annandale, NJ 08801, USA*
[c]*ExxonMobil Chemical Company, Baytown, TX 77520, USA*
[d]*Center for Neutron Research, National Institute of Standards and Technology, Gaithersburg, MD 20899, USA*
[e]*Department of Physics, North Carolina State University, Raleigh, NC 27695, USA*

Received 22 January 2001; received in revised form 3 April 2001; accepted 3 April 2001

Abstract

The interfacial properties of a homopolymer (polybutadiene (PB)) and a terpolymer (brominated poly(isobutylene-*co*-*p*-methylstyrene) (BIMS)) are reported. Neutron reflectivity was used to study the interfacial structure. The results were complemented by scanning transmission X-ray microscopy and atomic force microscopy, which were used to probe the morphology of these binary blends. Our results show that the interfacial behavior of these elastomeric blends is a direct function of the BIMS chemical composition. The interfacial width decreased with increasing bromide functionality. At levels below 8 mol%, the *para*-methylstyrene concentration had a less pronounced effect on the compatibility and interfacial characteristics. We also studied the effect of styrene butadiene random copolymers on the miscibility of the PB/BIMS blends. The results showed that styrene-butadiene rubber (SBR) was not fully miscible with BIMS and PB on an individual basis, but addition of relatively small amount of SBR enhances the compatibilization of the PB/BIMS interface. Self-consistent field (SCF) modeling was used to determine the optimum copolymer composition. The calculations are consistent with the experimental results.

Keywords: Polyolephin copolymers; Polymer blends; Polymer interfaces

1. Introduction

Good adhesion between chemically distinct elastomers is critical to the performance of elastomer blends and laminates in a wide variety of industrial applications [1]. It is well known that the mechanical properties of blends are directly related to their interfacial properties. For example, automobile tires have several laminated layers of rubber materials which are arranged in such a manner that the tire functions properly. Each layer has its own distinct mechanical and physical characteristics. The nature and physical properties of the interfacial structure are directly related to the chemical structure of the polymer or mixtures of polymers in each layer, e.g. butyl rubber, styrene-butadiene rubber, natural rubber, polyisoprene [2]. Hence, it is very important from technological point of view to probe the structure and dynamics of the interfacial region [3].

One of the new families of isobutylene-based elastomers is brominated poly(isobutylene-*co*-paramethylstyrene) (BIMS, Fig. 1(a)), a synthetic terpolymer of isobutylene (IB), *para*-methylstyrene (PMS) and *para*-bromomethylstyrene (BrPMS) [4]. The predominantly isobutylene-based terpolymer backbone is fully saturated which imparts high ozone and UV stability and impermeability to gases. The PMS component is used to control the modulus, and the reactive benzylic bromide group is the site for introducing unique chemical functionalities as well as chemical crosslinks, thus further increasing the control over physical properties. BIMS materials have numerous applications such as tire components, hoses, V-belts and vibration mountings [5].

Most applications require that general-purpose elastomers, such as polybutadiene, be blended with BIMS materials [6,7]. It is therefore important to understand how the variations of the PMS and BrPMS level affect the interfacial

* Corresponding author. Tel.: +1-908-730-2372; fax: +1-908-730-2536.
E-mail address: dgpeiff@erenj.com (D.G. Peiffer).

[1] Present address: Department of Chemistry, University of Saskatchewan, Saskatoon, Sask., Canada S7N 5C9.

0032-3861/01/$ - see front matter
PII: S0032-3861(01)00370-6

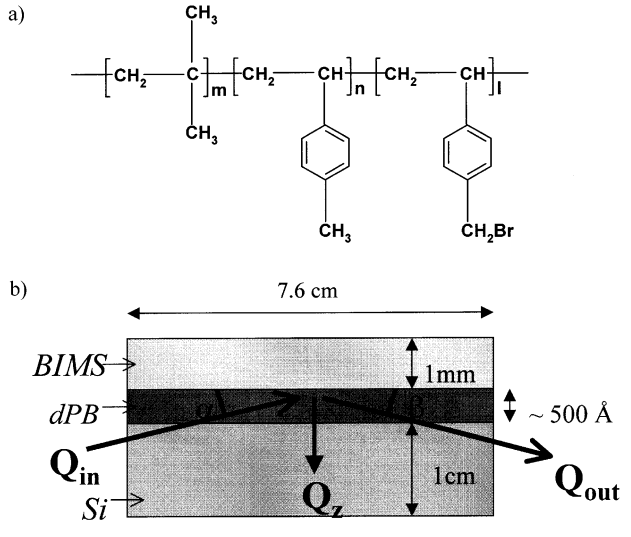

Fig. 1. (a) Molecular structure of BIMS, and (b) typical geometry of specular neutron reflectivity setup. The neutron beam enters through the silicon wafer in the Q_{in} direction, and is reflected from the dPB/BIMS interface in the Q_{out} direction.

properties. Furthermore, these applications also require that inexpensive compatibilizers exist for BIMS with various rubbers. The synthesis of grafts and other block copolymers is impractical. Hence, we also explored the potential of styrene-butadiene rubber (SBR), a random copolymer, as a compatibilizer. Self-consistent field (SCF) modeling is used to study the effect of SBR at the PB/BIMS interface, and to select an SBR with an optimum copolymer composition.

The technique we chose in this study is neutron reflectometry (NR), which is a powerful method to investigate polymer surface and interface behavior [8–14]. For the present system of elastomer materials, NR has two distinct advantages that make this approach the only possible technique to study these systems. First, the technique is non-destructive since long wavelength neutrons are used. Isobutylene-based polymers rapidly degrade under electron and ion bombardment [15]. Hence techniques such as dynamic secondary ion mass spectrometry (DSIMS) are not practical. Second, other techniques require the preparation of thin bilayer films. This is not possible for BIMS and other elastomers studied since their T_g's are below −20°C and the low viscosity at room temperature makes it impossible to float thin films. The samples can only be prepared as cast slabs that are too thick to be penetrated by charged particles such as electrons or ions. Therefore, NR is the method of choice that can probe the structure of the interfacial region between different elastomeric materials. We also describe the first use of a special chamber specifically designed for in situ NR measurements of compression molded rubber samples.

2. Experimental

2.1. Materials and sample preparation

The compositions and characteristic data of four BIMS terpolymers are listed in Table 1. The variation of PMS and BrPMS is minimal as controlled during the polymerization processes [5]. With up to 10 mol% PMS content, BIMS polymers are elastomeric in nature with low T_g's (−50°C). The polydispersity of these commercial BIMS polymers is in the range of 2.5–2.8. The characteristic data of deuterated polybutadiene (dPB), deuterated styrene-*co*-butadiene rubber (dSBR), and hydrogenated styrene-*co*-butadiene rubber (hSBR) used in this study are given in Table 2. BIMS terpolymers and hSBR were provided by Exxon Mobil, Baytown, TX. Deuterated polymers dPB and dSBR were purchased from Polymer Source, Montreal, Canada.

Both BIMS and dPB are elastomers with glass transition temperatures well below room temperature. To make standard large bilayer samples, conventional flotation techniques are not possible. Instead, we designed a special compression cell/mold to make disc-shaped BIMS pieces. For each sample, approximately 5 g of the BIMS material was molded at 150°C under a 3 metric ton load for one hour. Two polyimide sheets were used to protect the flat surfaces of the BIMS discs. In order to ensure a smooth surface, one polyimide sheet was removed just prior to the NR experiments by freezing the disc in liquid nitrogen and peeling off the polyimide layer.

Monodisperse dPB was dissolved in toluene and spin coated at 2500 rpm on 1 cm thick pre-cleaned silicon wafers (purchased from Wafer World, West Palm Beach, FL) of the same diameter as the BIMS discs. The dSBR and mixed dPB/hSBR (90/10 wt%) layers were prepared by a similar procedure. The thickness of resultant three dPB, two dSBR and three dPB/hSBR layers was measured with a Rudolph AutoEL Ellipsometer and listed in Table 3. These films were then pre-annealed at 120°C for one hour in a vacuum oven to relax any strains and to remove the solvent introduced from the spinning process. The thickness and roughness of these

Table 1
Isobutylene, total *p*-methylstyrene, *p*-bromomethylstyrene, and characteristics of four BIMS terpolymers used in this study

Polymer	PIB (mol%)	PMS (mol%)	BrPMS (mol%)	M_n (kg mol^{-1})	SLD (10^{-6} Å^{-2})
BIMS-1	93	6.9	0.75	189	− 0.21
BIMS-2	96	3.7	0.75	190	− 0.27
BIMS-3	96	3.7	1.20	154	− 0.27
BIMS-4	98	2.4	0.75	~ 160	− 0.29

Table 2
Characteristics of polymers (dPB, dSBR and hSBR) used in this study

Polymer	M_w (kg mol^{-1})	M_w/M_n	Styrene (%)	1,2-Linkage	T_g (°C)	SLD (10^{-6} Å^{-2})
dPB	223	1.03	–	0.10	< -20	6.35
dSBR	84	1.08	0.47	0.59	< -20	6.23
hSBR	105	2.69	0.24	0.20	< -20	0.62

layers were also characterized by the NG-7 reflectometer at the Center for Neutron Research (NCNR), the National Institute of Standards and Technology (NIST).

The dPB, dSBR and dPB/hSBR films on the silicon wafers were then sandwiched with the BIMS discs in a special press where a uniform tension could be applied across the entire sample. The magnitude of the tension was adjusted with a calibrated torque screwdriver so as to assure intimate contact of the dPB layer with the BIMS disc with minimal distortion of the BIMS layer.

In order to measure the inter-diffusion between the bilayer samples of various structures, the entire assembly in the press was placed in an oven and annealed in a vacuum of 10^{-3} Torr at 150°C for prescribed times. Since this temperature is well above the T_g of both polymers, a PTFE (polytetrafluoroethylene) ring attached to an adjustable clamp was used to maintain the shape of the disc and minimize the outward flow of the polymers during the annealing process. After annealing for prescribed times, the samples were quickly quenched in air to room temperature. This procedure took less than 5 min to complete. The sandwiched wafers were then mounted on the horizontal sample stage at the NG-7 reflectometer at NCNR, NIST. The geometry of the double layer sample and the neutron beam are shown in Fig. 1(b). In this study we examined eight double layer samples with compositions tabulated in Table 3. We will hereafter mention these bilayers as samples A through H.

The STXM samples were prepared by spin coating films of approximately 1200 Å thick on Si_3N_4 membranes. The Si_3N_4 membrane provides an X-ray transparent substrate to support the thin polymer layers for X-ray microscopy investigation. The resultant two films (50/50 wt% blend of dPB/BIMS-1 and 45/45/10 wt% blend of dPB/BIMS-1/SBR) were annealed in vacuum oven for 18 h at 150°C. The STXM experiment was performed on beamline X1A (X1A-STXM) at the National Synchrotron Light Source (NSLS) at Brookhaven National Laboratory (BNL).

Two atomic force microscopy (AFM) samples were spin coated from the same polymer solutions onto pre-cleaned silicon wafers and annealed in vacuum oven for 18 h at 150°C. The topography and lateral force of the surface were imaged with a DI3000 SFM (Nanoscope IIIa, Digital Instruments Co., Santa Barbara, CA) in the contact mode with a Si_3N_4 tip.

2.2. Scanning transmission X-ray microscopy technique

STXM has been used to study phase segregation in polymer blends [16,17]. The application of STXM to natural and synthetic polymers has been reviewed recently [18]. STXM experiment was performed using the Stony Brook STXM microscope at NSLS, BNL. Details about the instrument are described by Jacobsen et al. [19]. The STXM microscope uses diffractive focusing optics (a Fresnel zone plate) to produce a microprobe with a 35–50 nm diameter. An image is formed by measuring the transmitted X-ray signal as a thin sample section (typically ~100 nm thick) is raster scanned through the focus of a zone plate. The X-ray energy used for imaging can be chosen to correspond to discrete electronic transitions in the material, such as the C $1s \rightarrow \pi^*$C=C transition associated with C=C double bonds, which occurs at ~285 eV in most materials. At this energy, domains that have a higher concentration of C=C double bonds will appear darker in transmission microscopy, as more X-ray photons are absorbed. In blends

Table 3
Structure and composition of eight bilayer samples for NR experiment

Sample designation	First layer		Second layer		
	Polymer	Thickness (Å)	Polymer	Total PMS (mol%)	BrPMS (mol%)
A	dPB	508	BIMS-1	6.9	0.75
B	dPB	500	BIMS-2	3.7	0.75
C	dPB	500	BIMS-3	3.7	1.2
D	dSBR	570	BIMS-1	6.9	0.75
E	dSBR	570	BIMS-3	3.7	1.2
F	90/10 dPB/SBR	380	BIMS-1	6.9	0.75
G	90/10 dPB/SBR	570	BIMS-3	3.7	1.2
H	90/10 dPB/SBR	380	BIMS-4	2.4	0.75

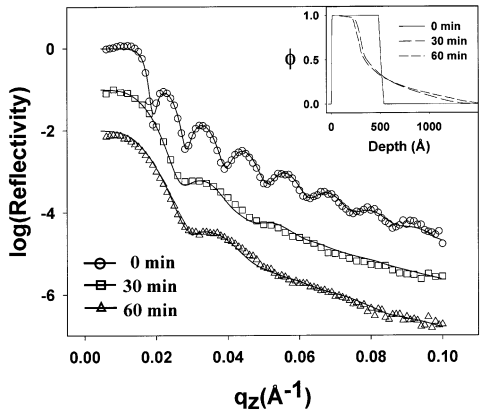

Fig. 2. Neutron reflectivity data (symbols) and best fits (solid lines) for different annealing times of the bilayer sample with a lower layer (dPB) 500 Å thick and an overlayer (BIMS-1) 1 mm thick. The inset shows best-fit profiles of dPB volume fraction as a function of distance from the silicon surface.

of dPB and BIMS imaged at this energy, the dPB domains will be dark relative to the BIMS domains.

3. Results and discussion

3.1. Neutron reflectivity

Fig. 2 shows the reflectivity profiles (R) obtained for a bilayer sample of dPB and BIMS with a low bromide (0.75 mol%) and high PMS (6.9 mol%) content (sample A), after annealing at 150°C for different times. The data are plotted as log R vs. Q_z, where $Q_z = (4\pi/\lambda)\sin\theta$, and Q_z, λ and θ are the incident neutron wave vector, neutron wavelength, and incident angle, respectively. Further details on the technique can be found in a review by Russell [8,9]. The curves in all the reflectivity figures are vertically shifted for clarity. From the plot of the data for the unannealed sample we can see well-defined Kessig oscillations, which indicate

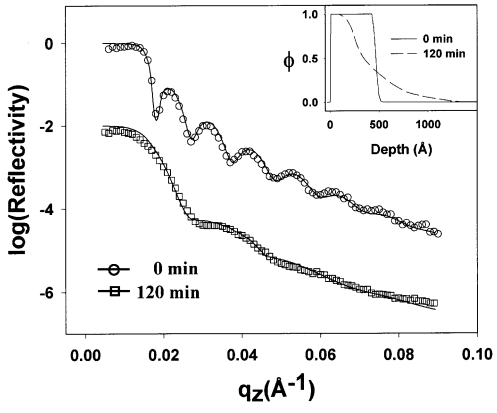

Fig. 3. Neutron reflectivity data (symbols) and best fits (solid lines) for different annealing times of the bilayer sample with a lower layer (dPB) 500 Å thick and an overlayer (BIMS-2) 1 mm thick. The inset shows best-fit profiles of dPB volume fraction as a function of distance from the silicon surface.

that the dPB/BIMS interface is sharp. This proves that the method of sample preparation was successful.

The 0 min curve is fit by a single layer model of dPB with an error function interface with the BIMS, which is assumed to be an infinite medium. The parameters used in the fitting are described as follows. The thickness of the dPB layer (d_1), the PB/BIMS interfacial width (w), the thickness of SiO_2 layer (d_2), Si/SiO_2 roughness (σ_1), and SiO_2/dPB roughness (σ_2). The SLD values of the polymers were listed in Tables 1 and 2. It should be noted that the reflectivity curve is determined primarily by d_1 and w in this system. Due to the HF treatment, the values of σ_1, σ_2 and d_2 are very small, i.e. typically 6, 6 and 15 Å, respectively. As can be seen in the inset, the data is well fitted with a dPB layer of thickness $d_1 = 494$ Å. The dPB/BIMS interface is well fitted by an error function of width $w = 30$ Å. After annealing for 30 min at 150°C, the amplitude of the oscillations decreases, indicating that the interface is becoming more diffuse. The remnant low frequency oscillation indicates that only part of the dPB layer has diffused into the BIMS. In order to fit this oscillation it was necessary to add another dPB layer of thickness d_0 and that was immobilized at the substrate. This asymmetric dPB volume fraction profile was found to produce a better fit to the reflectivity data at high Q_z than a symmetric profile. The asymmetry is partially due to the adsorbed layer and the fact that the BIMS has a relatively large polydispersity. Annealing for 60 min further decreases the remnant frequency indicating that the adsorbed layer is becoming somewhat thinner, but still distinct from the rest of the layer. The inset shows the dPB volume fraction profiles that were found to produce the best fits to the data of the annealed samples. Since reflectivity measurements are only sensitive to the amplitude of the scattered intensity and not the phase, it is not possible to obtain unique fits to the data. In order to reduce the number of possibilities, other constraints from complementary measurements are introduced. In this case the total thickness of the dPB layer and the oxide layer are known from ellipsometry and X-ray reflectivity. Therefore the volume fraction profiles shown in the inset are constrained to conserve the total integrated initial volume of dPB. The oscillations in the data unambiguously determine the thickness of the flat portions in the concentration profile, whereas the fall-off of intensity at higher values of Q_z indicates a broad interface, but is not sensitive to the exact functional form at the interface. For symmetric fraction profiles the interfacial width w is defined as:

$$w = (\partial\phi/\partial x)^{-1}_{x=0} \tag{1}$$

where ϕ is the volume fraction, and $x = 0$ is the center of the interface such that $\phi_{(x=0)} = 0.5$.

For diffused volume fraction profiles with asymmetric polymer/polymer interfaces as shown in the inset, the interquartile width [20], i.e. the distance between $\phi =$ 1/4 and 3/4 concentration points, was measured and

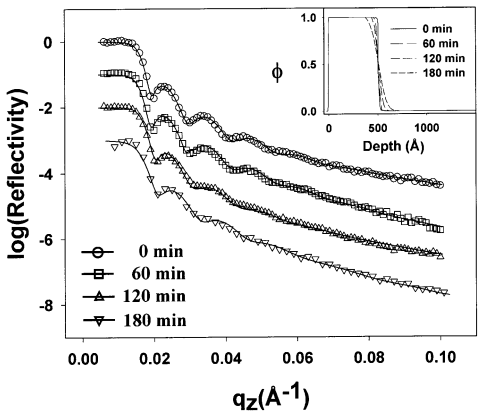

Fig. 4. Neutron reflectivity data (symbols) and best fits (solid lines) for different annealing times of the bilayer sample with a lower layer (dPB) 500 Å thick and an overlayer (BIMS-3) 1 mm thick. The inset shows best-fit profiles of dPB volume fraction as a function of distance from the silicon surface.

regarded as the interfacial width (w) between dPB and BIMS.

Although the initial interfacial width prior to annealing is quite narrow ($w = 30$ Å), the dPB/BIMS interface broadens significantly after 30 min of annealing. The biggest change occurred between 0 and 30 min, and further annealing to 60 does not change the interfacial structure, indicating that an equilibrium configuration is achieved. This is further confirmed by the fact that the profile remains unchanged even after annealing for 420 min (not shown). The main difference between the profiles at 30 and 60 min is the position of the first minimum of a remnant oscillation, which decays at higher Q_z values. We interpret this oscillation as being due to a layer of dPB adsorbed to the silicon substrate. Diffusion away form this layer is significantly slowed down due to interactions with the substrate. The 'equilibrium' value for this adsorbed layer achieved after 210 min of annealing, 145 Å, is comparable to the radius of gyration, R_g, of dPB polymer. The equilibrium PB/BIMS interface w is approximately 340 Å.

Fig. 3 shows the reflectivity profiles obtained for sample B, in which the BIMS layer has the same level of bromide (0.75 mol%) as sample A, but the concentration of PMS has been reduced (3.7 mol%). The initial thickness of the dPB layer is comparable to sample A. From the figure we can see that the reflectivity spectrum for samples annealed for 120 min looks similar to that shown in Fig. 2 (sample A), indicating that in this case as well there is a thin layer of dPB strongly adsorbed on the substrate. The inset shows that the initial sharp interface of 30 Å broadens to approximately 350 Å after 120 min of annealing.

The reflectivity profiles of sample C are shown in Fig. 4. In sample C, the BIMS layer has the same level of PMS (3.7 mol%) as in sample B, but the level of bromide has been increased (1.2 mol%). This is markedly higher than the amount contained in samples A and B (0.75 mol%). From the figure we can see that there is little change in the reflectivity spectra between annealed and unannealed samples, or the interface remains narrow. The fits in the inset indicate a consistently sharp volume fraction profile of dPB layer with an interface $w = 70$ Å that persists even after 3 h of annealing. From these spectra we see that the interfacial width is very sensitive to changes in bromide content, and rather insensitive to changes in PMS content in the range below 7 mol%. The Flory–Huggins parameter χ for the three pairs of dPB/BIMS samples can be estimated from the interfacial measurement using the following equation:

$$w = \left[\frac{4a^2}{6\chi} + \frac{a^2}{2\pi}\sqrt{\frac{6}{\chi}}\ln\left(\frac{\lambda_{max}}{\lambda_{min}}\right)\right]^{1/2}\left[1 + \frac{\ln 2}{\chi}\left(\frac{1}{N_A} + \frac{1}{N_B}\right)\right] \quad (2)$$

where w is the equilibrium interfacial width,[2] a the statistical segment length (approximately 7 Å), λ_{max} is the coherence length of neutron beam (estimated as 10,000 Å) and λ_{min} is the intrinsic interfacial width (estimated as 5 Å). The second part in the first term is a correction for capillary wave effect [21], and the second term is for chain length effect [22]. N_A and N_B are the degrees of polymerization of PB and BIMS. The obtained χ values are listed in Table 4. We can clearly see that the polymer pair in sample C (dPB/BIMS-3) is significantly more immiscible than those in samples A and B. The strong effect of the benzylic bromide functionality on miscibility may in part be attributed to the size and the polar nature of the BrPMS group which will interact unfavorably with the completely nonpolar polybutadiene layer. The relatively low level of BrPMS functionality may impart large changes in physical and chemical properties. This effect has been observed in many similar occasions before. For example, the attachment of low levels of associating groups such as sulfonate groups (<1 mol%) to a polymer chain produces materials with markedly different bulk and solution properties [23,24].

Table 4
The Flory–Huggins parameters χ of three binary blends of dPB/BIMS and two binary blends of BIMS/dSBR

Sample designation	Polymer A	Polymer B	χ
A	dPB	BIMS-1	0.00053
B	dPB	BIMS-2	0.00062
C	dPB	BIMS-3	0.0103
D	dSBR	BIMS-1	0.0038
E	dSBR	BIMS-3	0.0018

[2] Due to the complexity of the volume fraction profiles of dPB at the PB/BIMS interface, the distance between the $\Phi = 1/4$ and 3/4 concentration points, was measured as the interfacial width for PB/BIMS-1 and PB/BIMS-2 pairs; $w = (\partial\Phi/\partial x)^{-1}_{x=0}$ was calculated for PB/BIMS-3 pair.

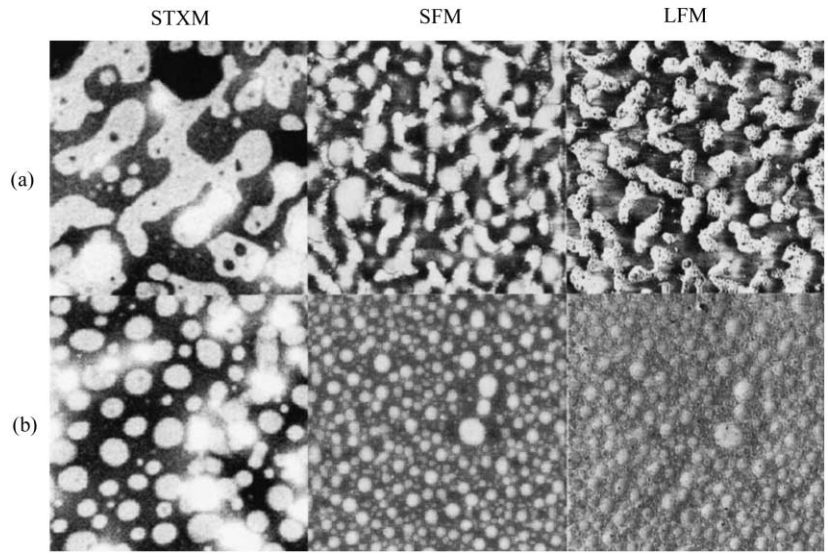

Fig. 5. STXM (10 μm × 10 μm), SFM and LFM (both 30 μm × 30 μm) scans of blend films consist of: (a) dPB/BIMS-1 (50/50 wt%) and (b) dPB/BIMS-1/hSBR (45/45/10 wt%). The films, approximately 1200 Å thick, were annealed in vacuum for 18 h at 150°C. The dark areas in the STXM scans correspond to the dPB phase.

3.2. Scanning transmission X-ray microscopy and atomic force microscopy

The immiscibility of BIMS and dPB is also manifested when the two components are blended in solution and spun cast on a Si_3N_4 or silicon substrate. The morphology of the films can be observed by STXM and AFM. The STXM scan of the 50/50 wt% dPB/BIMS-1 blend annealed for 18 h at 150°C is shown in Fig. 5(a). The dark areas in the figure correspond to the intensity of the 285 eV $C1_s \rightarrow \pi^*_{C=C}$ absorption in dPB. From the figure we can see that phase segregation has occurred after annealing for 18 h at 150°C. PB is observed to wet the substrate while BIMS dewets the PB layer. Fig. 5(a) also shows the scanning force microscopy (SFM) and lateral force microscopy (LFM) image of the same 50/50 wt% blend of dPB/BIMS-1 annealed at 150°C for 18 h on a silicon substrate. The small contact angle, $\theta = 6°$, is consistent with the broad interface observed in the NR experiment. When the substrate layer is sufficiently thin, the interfacial force $\gamma_{A/B}$ can be estimated by the classical Young's relationship:

$$\gamma_A - (\gamma_{A/B} + \gamma_B \cos\theta) = 0 \quad (3)$$

where γ_A and γ_B, both approximately 24 dyne cm^{-1},[3] are the surface energies of dPB and BIMS, and θ is the angle formed on a dPB surface by a BIMS droplet at equilibrium conditions. The Flory–Huggins parameter χ can then be estimated from the relationship of Helfand [25,26]:

$$\gamma_{A/B} = a\rho k_B T(\chi/6)^{1/2} \quad (4)$$

where a is the monomer length (estimated as 7 Å), $1/\rho$ the monomer volume, and T the temperature. The resultant $\chi = 0.00073$ is consistent with $\chi = 0.00053$ obtained from the NR experiments.

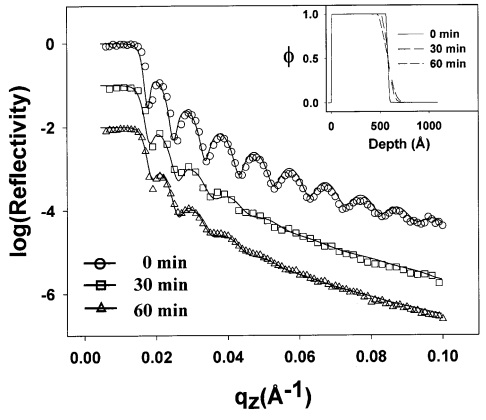

Fig. 6. Neutron reflectivity data (symbols) and best fits (solid lines) for different annealing times of the bilayer sample with a lower layer (dSBR) 570 Å thick and an overlayer (BIMS-1) 1 mm thick. The inset shows best-fit profiles of dPB volume fraction as a function of distance from the silicon surface.

3.3. Compatibilization of BIMS/butadiene blends

SBR has been used extensively in rubber blends [27,28]. We therefore decided to explore its ability to compatibilize the dPB/BIMS blend system. We first explored the miscibility of BIMS and SBR. Two 570 Å thick dSBR layers were spun cast on a silicon wafer and sandwiched with two BIMS discs with low and high BrPMS (0.75 and 1.2 mol%) but the same PMS (6.9 mol%) content. The neutron reflectivity profiles and best fits for samples

[3] Data from Bryan B. Sauer. Private communication.

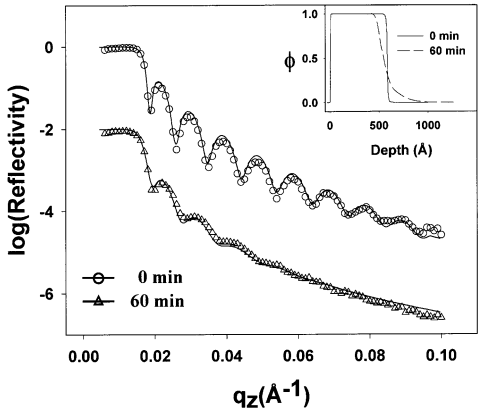

Fig. 7. Neutron reflectivity data (symbols) and best fits (solid lines) for different annealing times of the bilayer sample with a lower layer (dSBR) 570 Å thick and an overlayer (BIMS-3) 1 mm thick. The inset shows best-fit profiles of dPB volume fraction as a function of distance from the silicon surface.

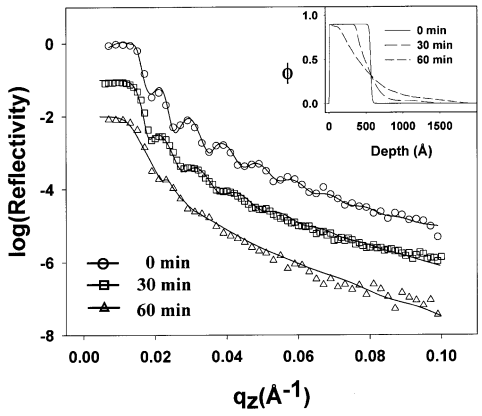

Fig. 9. Neutron reflectivity data (symbols) and best fits (solid lines) for different annealing times of the bilayer sample with a lower layer (90/10 wt% mixture of dPB/SBR) of 570 Å and an overlayer (BIMS-3) of 1 mm. The inset shows best-fit profiles dPB volume fraction as a function of distance from the silicon surface.

annealed at 150°C for various times are shown in Figs. 6 and 7. From the figures we can see that in contrast to the dPB/BIMS blends, the interfacial widths of BIMS/SBR are comparable for both BIMS and hence χ is less sensitive to the bromide content. The χ values were estimated using Eq. (2), and were listed in Table 4. These values are intermediate between these for dPB and BIMS with high and low bromide content. The interfacial properties of the SBR polymer were probed by spin casting a film with a blend of 10% hSBR and 90% dPB. The films were then sandwiched with BIMS of different bromide and PMS content. Fig. 8 shows the reflectivity profiles and associated model fits for the bilayer of BIMS-1 and the hSBR/dPB blend (sample F). As was observed previously, the unannealed sample has a sharp interface and well-defined oscillations. After 30 min the interface broadens to 200 Å and continues to broaden after further annealing for 60 min. Since the intensity drops as the interface is progressively broadened,

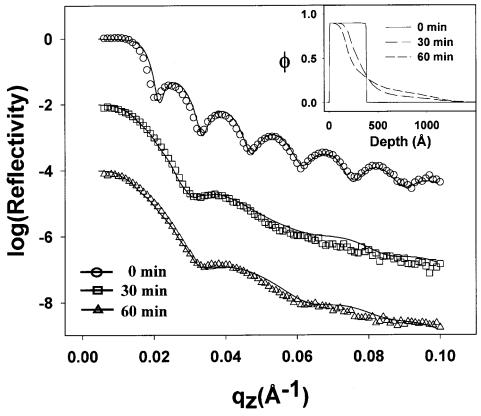

Fig. 8. Neutron reflectivity data (symbols) and best fits (solid lines) for different annealing times of the bilayer sample with a lower layer (90/10 wt% mixture of dPB/SBR) of 380 Å and an overlayer (BIMS-1) of 1 mm. The inset shows best-fit profiles of dPB volume fraction as a function of distance from the silicon surface.

we could not determine if the interfacial width has reached equilibrium yet. Similar results were also obtained for the sample with BIMS having the same bromide content, but lower PMS (2.4 mol%) fraction (sample G, data not shown).

Fig. 9 shows the reflectivity profiles obtained for sample H, in which the BIMS layer has the same high bromide amount (1.2 mol%) as in sample C (Fig. 4), while the first layer is a 90/10 wt% blend of dPB/SBR. The reflectivity curve of the unannealed sample has well-defined oscillations. After 30 min of annealing, the amplitude of the oscillations was markedly reduced, indicating the interface became wide. After 60 min of annealing, most of the fringes vanished. The fits in the inset show that the interface is broadened to 440 Å after 60 min. Comparing these data with the narrow interfacial profile shown in Fig. 4, we can derive that the addition of SBR decreased the interfacial tension from 0.47 to 0.11 dyne cm^{-1}, using Eqs. (2) and (4). Furthermore, the effectiveness of SBR as a compatibilizer seems to be independent of the bromide or PMS content of the BIMS.

The effectiveness of SBR as a compatibilizer can also be observed directly form the changes in the morphology of blend films. Fig. 5(b) shows the STXM image of a spin cast film containing a 45/45/10 wt% blend of SBR, dPB and BIMS-1. Comparing the two STXM images in Fig. 5 we can see that addition of the SBR copolymer has significantly reduced the size of the BIMS domains. The AFM scans of the same film in Fig. 5(b) indicate that the contact angle between two phases is now approximately 4°. This translates into a reduction of the interfacial tension from 0.13 to 0.06 dyne cm^{-1} as 10 wt% of SBR is included. The creation of excess interfacial area, as well as the reduction in the contact angle are consistent with the broad interface measured with NR.

3.4. Self-consistent mean field model

3.4.1. Determination of Flory–Huggins parameters

The NR results can be compared with Self-consistent

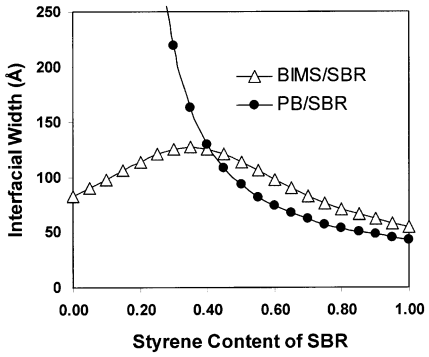

Fig. 10. Interfacial width of BIMS/SBR (triangle) and PB/SBR (circle) plotted vs. styrene content Φ of SBR. The 1,2-linkage content of SBR is 0.2.

mean field (SCF) calculation for an A/B system with a BC compatibilizer. We chose the bilayer samples with the high bromide content (Figs. 4 and 7), since the compatibilization is most dramatic. As listed in Table 4, the effective Flory–Huggins parameters[4] of dPB/BIMS-3 and BIMS-3/dSBR are $\chi_1 = 0.0103$ and $\chi_2 = 0.0018$. Hereafter, the symbols of χ_1, χ_2 and χ_3 are used to describe the effective Flory–Huggins parameters for the PB/BIMS, BIMS/SBR, and PB/SBR pairs, respectively.

We use a random copolymer theory developed by Brinke et al. [29] and Paul et al. [30] to obtain the values of χ_2 as a function of the styrene content (Φ) of SBR. The details of the calculation are described elsewhere [31]. Here we only present the results:

$$\chi_2 = 0.0098 - 0.027\Phi + 0.039\Phi^2 \quad (5)$$

The χ_3 values as a function of Φ were derived from the result of Sakurai et al. [32]

$$\chi_3 = 0.00007 - 0.0033\Phi + 0.039\Phi^2 \quad (6)$$

On the basis of Eqs. (5) and (6), the calculated interfacial widths of BIMS-3/SBR and PB/SBR for the PB/BIMS-3/SBR blend at different styrene content Φ are plotted and shown in Fig. 11. These results are used in the initial analysis of SCF modeling described later.

3.4.2. Modeling results

Self-consistent mean field (SCF) lattice model, developed by Scheutjens and Fleer [33], was modified to determine the properties of polymer blend system. One dimensional lattice model is used in this calculation. The calculation yields density profiles for the polymers in the lowest free energy state. These density profiles provide information on the location of the polymer interfacial agent and the width of the interface. These calculations also allow the determination of interfacial tension. Only the final results are presented here. Interested readers are referred to the literature [34] for a more detailed description.

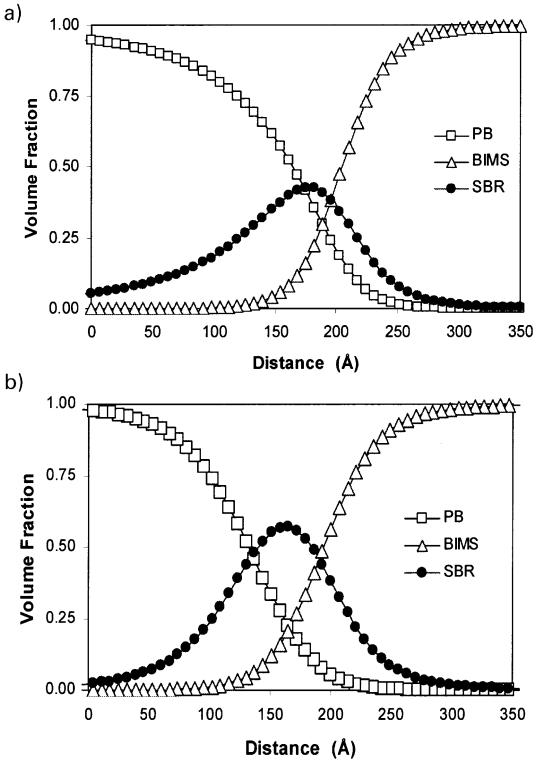

Fig. 11. Volume fraction profiles of a three-phase system of PB (square), BIMS (triangle), and SBR (circle) of (a) 25% styrene and (b) 35% styrene.

In this system, we consider how the styrene content (Φ) affects the values of χ_2 and χ_3, and subsequently the interfacial widths of BIMS/SBR and PB/SBR. In order to determine the choice of compositions to be studied by the model, we used the interfacial width of BIMS-3/SBR and PB/SBR at different styrene content Φ, as shown in Fig. 10. It is obvious from Fig. 10 that either BIMS/SBR or PB/SBR interface will be narrow if Φ is less than 20% or over 50%. This allows us to limit the range of Φ to be studied. In the calculation presented here we first chose Φ similar to that of the NR experiment, i.e. 25%. The composition of PB/SBR/BIMS is 45/5/50, which is similar to the NR experiment. From the result shown in Fig. 11(a), SBR is seen to localize at the PB/BIMS interface with an asymmetric profile. SBR has a broader overlap with the PB phase, indicating higher miscibility of PB/SBR. The final interfacial width of PB for this system is 210 Å assuming a statistical segment length of 7 Å. This is approximately three times of the interfacial width (70 Å) of the binary system dPB/BIMS-3, in which SBR is not present. The large increase of interfacial width is consistent with the experimental width determined by NR. Two more systems with SBR structures of 35 and 45% styrene were also calculated. As shown in Fig. 11(b), the SBR profile with 35% styrene is

[4] On the basis of copolymer blend theory, the term effective Flory–Huggins parameter refers to the weighted sum of fundamental segmental interaction parameters between different repeating units, if BIMS-3 and dPB are considered as random copolymers. Details can be found in Refs. [29–32].

nearly symmetric due to the comparable miscibility of PB/SBR and BIMS/SBR at this styrene level, i.e. $\chi_3 \approx \chi_2$. Increasing the styrene content of SBR from 35 to 45% narrows the interface of PB by 30 Å. In general, addition of SBR in the system compatibilizes the PB/BIMS system by increasing the overlap of both PB and BIMS.

The divergence of calculated interfacial width (210 Å) from the experimental value (440 Å) may be due to the fact that both BIMS and SBR are industrial materials with polydispersity of 2.7. Lower molecular weight chains tend to segregate to the interface, hence the observed interface is wider than calculated, where all polymers are assumed to be monodisperse. In addition, the polydispersity also produces asymmetric interfacial profiles. This introduces an underestimation of the interfacial width. Studies which incorporate this polydispersity are currently underway.

4. Conclusions

We have demonstrated that it is possible to use neutron reflectivity to study the interfacial properties of thick, molded rubber materials. In this study the inherent difficulties in floating low glass transition temperature materials were overcome by the use of a specially designed mold and press sample holder. Utilizing this technique we were able to produce elastomeric layers having a sharp interface, which is the appropriate starting point for successfully following and monitoring the interfacial diffusion of these elastomers. Prior to the thermal treatment the interface between the two elastomeric materials was very sharp. The analysis of the initial data clearly confirms that little, if any, material has diffused across the interface. However, with minimal thermal treatment the interface begins to become more diffusive as indicated by the marked changes in the reflectivity curves as a function of the annealing time. The reflectivity data is used to determine the change in the structure and dynamics occurring at the interface.

Although the thickness of the dPB layer is approximately 500 Å for all samples, the variation of the monomer composition in the BIMS phase affects the interfacial behavior significantly. In general, the rate of interface diffusion is strongly dependent on the bromide level and relatively independent on the PMS level. The precise mechanism for this behavior is not completely understood, but it appears to be related to the large size of the bromide group as well as to its polarity. Since polybutadiene is nonpolar, the degree of compatibility and therefore the equilibrium interfacial width should become lower with higher levels of the polar functionality.

The interfacial width of BIMS and SBR is not strongly affected by the bromide level of BIMS terpolymers, as observed by NR experiment. SBR copolymers partially resemble PB and BIMS polymers. Although SBR is not fully miscible with BIMS and PB individually, as observed in the NR experiment, 10 wt% of SBR compatibilizes the PB/BIMS interface significantly, as observed by NR, STXM and AFM experiments.

SCF studies indicate that the PB/BIMS/SBR blend can also be studied by a random copolymer theory coupled with SCF modeling. The result of SCF modeling on this specific system (PB/BIMS-3/SBR) is consistent with the experimental results.

Acknowledgements

This work was supported by NSF MRSEC program No. DMR96325235. H.A. and S.G.U. are supported by NSF Young Investigator Award No. DMR9458060.

References

[1] Brown HR. IBM J Res Dev 1994;38(4):379.
[2] Zhu SH, Chan CM. Macromolecules 1998;31:1690.
[3] Lee LH. Adhesives engineering 1993; SPIE 1999:6.
[4] Rogers JE, Waddell WH. Rubber World 1999:24.
[5] Wang HC, Powers KW. Elastomerics 1992;February:22.
[6] Gursky LJ, Fusco JV, Flowers DD. US Patent 5,532,312, 1996.
[7] Costemalle B, Flowers DD, Fusco JV, Steurs M. US Patent 5,376,438, 1994.
[8] Russell TP. Mater Sci Rep 1990;5:171.
[9] Russell TP. Physica B 1996;221:267.
[10] Bucknall DG, Butler SA, Higgins JS. Macromolecules 1999;32:5453.
[11] Kunz K, Stamm M. Macromolecules 1996;29:2548.
[12] Lin EK, Kolb R, Satija SK, Wu WL. Macromolecules 1999;32:3753.
[13] Wu WL, Wallace WE, Van Zanten JH, Bauer BJ, Liu DW, Wong A. Polymer 1997;38(11):2583.
[14] Feng Y, Weiss RA, Karim A, Han CC, Ankner JF, Kaiser H, Peiffer DG. Macromolecules 1996;29:3918.
[15] Galuska A, Poulter R, McElrath KO. Surf Interf Anal 1997; 25(6):418.
[16] Zhu S, Liu Y, Rafailovich MH, Sokolov J, Gersappe D, Winesett DA, Ade H. Nature 1999;400:49.
[17] Ade H, Winesett DA, Smith AP, Qu S, Ge S, Rafailovich MH, Sokolov S. Europhys Lett 1999;45:526.
[18] Ade H, Urquhart SG. In: Sham TK, editor. Chemical applications of synchrotron radiation. Singapore: World Scientific, 2001, in press.
[19] Jacobsen C, Williams S, Anderson E, Brown MT, Buckley CJ, Kern D, Kirz J, Rivers M, Zhang X. Opt Commun 1991;86:351.
[20] Jordan EA, Ball RC, Donald AM, Fetters LJ, Jones RAL, Klein J. Macromolecules 1988;21:235.
[21] Shull KR, Mayes AM, Russell TP. Macromolecules 1993;26:3929.
[22] Broseta D, Fredrickson GH, Helfand E, Leibler L. Macromolecules 1990;23:132.
[23] Lundberg RD, Makowski HS. J Polym Sci, Polym Phys Ed 1980;18:1821.
[24] Lundberg RD, Phillips RR. J Polym Sci, Polym Phys Ed 1982;20:1143.
[25] Helfand E, Tagami Y. Polym Lett 1971;9:741.
[26] Helfand E, Tagami Y. J Chem Phys 1972;56:3592.
[27] Powers KW, Wang HC, Chung TC, Dias AJ, Olkusz JA. US Patent 5,162,445, 1992.
[28] Zhu SH, Chan CM. Polymer 1998;39:7023.
[29] Ten Brinke G, Karasz FE, MacKnight WJ. Macromolecules 1983;16:1827.
[30] Paul DR, Barlow JW. Polymer 1984;25:487.
[31] Zhang Y. PhD Thesis. Stony Brook: SUNY; 2000.
[32] Sakurai S, Izumitani T, Hasegawa H, Hashimoto T, Han CC. Macromolecules 1991;24:4844.
[33] Scheutjens JMHM, Fleer GJ. J Phys Chem 1979;83:1619.
[34] Evers OA, Scheutjens JMHM, Fleer GJ. Macromolecules 1990;23:5221.